

High-pressure studies on quasi-one-dimensional systems

Wenhui Liu(刘雯慧), Jiajia Feng(冯嘉嘉), Wei Zhou(周苇), Sheng Li(李升), and Zhixiang Shi(施智祥)
Citation: Chin. Phys. B, 2025, 34 (**8**): 088104. DOI: 10.1088/1674-1056/ade8dd
http://cpb.iphy.ac.cn; http://iopscience.iop.org/cpb

What follows is a list of articles you may be interested in

Screening *A*-site ordered quadruple perovskites for alkaline hydrogen evolution reaction via unifying electronic configuration descriptor

Ning Sun(孙宁), Wenbo Li(李文博), Yang Qin(秦杨), Zhichuan Zheng(郑智钏), Bowen Zhang(张博文), Xiangjiang Dong(董祥江), Peng Wei(魏鹏), Yixiao Zhang(张艺潇), Xian He(何贤), Xinyu Xie(谢新煜), Kai Huang(黄凯), Lailei Wu(吴来磊), Ming Lei(雷鸣), Huiyang Gou(缑慧阳), and Runze Yu(于润泽)
Chin. Phys. B, 2024, 33 (**12**): 128101. DOI: 10.1088/1674-1056/ad8074

Structural behavior and metallization of $AsSbS_3$ at high pressure

Tian Qin(覃天), Min Wu(武敏), Kai Wang(王凯), Ye Wu(吴也), and Haijun Huang(黄海军)
Chin. Phys. B, 2024, 33 (**11**): 118101. DOI: 10.1088/1674-1056/ad78d8

Recension of boron nitride phase diagram based on high-pressure and high-temperature experiments

Ruike Zhang(张瑞柯), Ruiang Guo(郭睿昂), Qian Li(李倩), Shuaiqi Li(李帅琦), Haidong Long(龙海东), and Duanwei He(贺端威)
Chin. Phys. B, 2024, 33 (**10**): 108103. DOI: 10.1088/1674-1056/ad6a06

Pressure generation under deformation in a large-volume press

Saisai Wang(王赛赛), Xinyu Zhao(赵鑫宇), Kuo Hu(胡阔), Bingtao Feng(丰丙涛), Xuyuan Hou(侯旭远), Yiming Zhang(张羿鸣), Shucheng Liu(刘书成), Yuchen Shang(尚宇琛), Zhaodong Liu(刘兆东), Mingguang Yao(姚明光), and Bingbing Liu(刘冰冰)
Chin. Phys. B, 2024, 33 (**9**): 098104. DOI: 10.1088/1674-1056/ad58c6

High-pressure and high-temperature sintering of pure cubic silicon carbide: A study on stress-strain and densification

Jin-Xin Liu(刘金鑫), Fang Peng(彭放), Guo-Long Ma(马国龙), Wen-Jia Liang(梁文嘉), Rui-Qi He(何瑞琦), Shi-Xue Guan(管诗雪), Yue Tang(唐越), and Xiao-Jun Xiang(向晓君)
Chin. Phys. B, 2023, 32 (**9**): 098101. DOI: 10.1088/1674-1056/aca6d4

TOPICAL REVIEW — Structures and properties of materials under high pressure

High-pressure studies on quasi-one-dimensional systems

Wenhui Liu(刘雯慧)[1,2], Jiajia Feng(冯嘉嘉)[3], Wei Zhou(周苇)[4], Sheng Li(李升)[1,5,6,†], and Zhixiang Shi(施智祥)[1,6,‡]

[1] *School of Physics, Southeast University, Nanjing* 211189, *China*
[2] *Institute of Quantum Materials and Physics, Henan Academy of Sciences, Zhengzhou* 450046, *China*
[3] *Center for High Pressure Science and Technology Advanced Research (HPSTAR), Beijing* 100094, *China*
[4] *School of Electronic and Information Engineering, Changshu Institute of Technology, Changshu* 215500, *China*
[5] *Purple Mountain Laboratories, Nanjing* 211111, *China*
[6] *Key Laboratory of Quantum Materials and Devices of Ministry of Education, School of Physics, Southeast University, Nanjing* 211189, *China*

(Received 25 March 2025; revised manuscript received 26 May 2025; accepted manuscript online 27 June 2025)

Quasi-one-dimensional systems provide a unique platform for the exploration of novel quantum states due to their enhanced electronic correlations, strong anisotropy, and dimensional confinement. Among various external tuning methods, physical pressure has been experimentally demonstrated to be an exceptionally potent and precise method for modulating both the structural and electronic properties of quasi-one-dimensional systems. In this review, we focus on the application of pressure to construct pressure-temperature phase diagrams of quasi-one-dimensional materials and explore the intricate relationships among quantum phenomena between superconductivity and other electronic states, such as charge density wave, topological quantum states, and antiferromagnetism. By analyzing representative examples across distinct material families, we demonstrate how pressure can be used not only to induce superconductivity but also to reveal underlying quantum critical points and drive topological phase transitions. We emphasize the significant potential of pressure as a crucial tuning parameter for revealing novel quantum phenomena and driving the progress in advanced low-dimensional quantum materials.

Keywords: high pressure, quasi-one-dimensional system, superconductivity

PACS: 81.40.Vw, 74.62.Fj, 61.50.Ks

DOI: 10.1088/1674-1056/ade8dd **CSTR:** 32038.14.CPB.ade8dd

1. Introduction

Quasi-one-dimensional (quasi-1D) systems are fascinating for exploring emergent quantum phenomena, as they retain the strong electronic correlations and van Hove singularities arising from the flat band of purely one-dimensional (1D) systems while introducing interchain coupling effects in real materials. In contrast to high dimensional systems, low-energy particle-hole pairs are only excited in 1D systems when the wave vector $|q| \sim 0$ or $|q| \sim 2k_F$, where k_F is the Fermi momentum (see Fig. 1).[1] The reduction of electron scattering in momentum space and the effects of electron screening collectively give rise to phenomena such as power-law correlation functions and collective excitations associated with spin-charge separation, as described by Tomonaga–Luttinger liquid (LL) theory.[2] Low-energy excitations are no longer the simultaneous transmission of charge and spin. Instead, they are independently separated into spin excitations (spinons) and charge excitations (holons).

Although ideal 1D systems are rarely realized in real materials, many quasi-1D compounds with chain-like atomic or molecular arrangements can closely emulate the physical behavior of ideal 1D systems. In these materials, the intrachain electron interactions are much stronger than the weak van der Waals interactions between the quasi-one-dimensional chains, resulting in pronounced anisotropy.[3] Electron motion is predominantly confined to a specific direction, which significantly amplifies low-dimensional quantum phenomena such as the quantum size effect and quantum tunneling.[1] Despite the presence of interchain coupling, the reduced dimensionality of these systems significantly enhances electron correlations and quantum fluctuations, often exceeding those found in two- or three-dimensional systems. Due to the coexistence of strong electron–phonon coupling and electron correlation, quasi-1D materials exhibit various quantum ordered states, such as charge density wave (CDW), spin density wave (SDW), novel topological phases, exotic magnetism, and superconductivity, which provide a perfect platform for the study of quantum physics.[4–9]

In quasi-1D compounds, CDW instability and Peierls transition often occur when the electron density along the chain direction adopts a periodicity that deviates from the lattice periodicity.[10,11] In systems containing transition metal

†Corresponding author. E-mail: sheng_li@seu.edu.cn
‡Corresponding author. E-mail: zxshi@seu.edu.cn

© 2025 Chinese Physical Society and IOP Publishing Ltd. All rights, including for text and data mining, AI training, and similar technologies, are reserved.

or rare-earth elements with partially filled d or f orbitals, due to the influence of frustration and pronounced anisotropy, the mechanism for achieving the quantum ground state becomes more complex with phase diversity and often leads to unique physical phenomena, such as SDW, magnetic solitons, and quantum spin liquids.[12–14] At the same time, the spin structure of quasi-1D spin chain materials is also influenced by low-dimensional quantum fluctuations and exchange interactions, presenting various magnetic ground states including antiferromagnetic (AFM) order and incommensurate magnetic structures.[15–20] Under the regulation of external fields, the spins can be driven to rotate, leading to the emergence of novel quantum phenomena including spin flip transition and spin triplet superconductivity.[21] In recent years, the discovery of quasi-1D topological materials provides new perspectives for exploring electron ordering and quantum phase transitions due to the unique topological protection boundary states and electronic structures.[8,22–24] Furthermore, many quasi-1D materials exhibit superconductivity at low temperatures, and the superconducting mechanism may involve unconventional superconducting pairing, which could be attributed to the dimensionality-induced effect and enhanced electron correlations.[25]

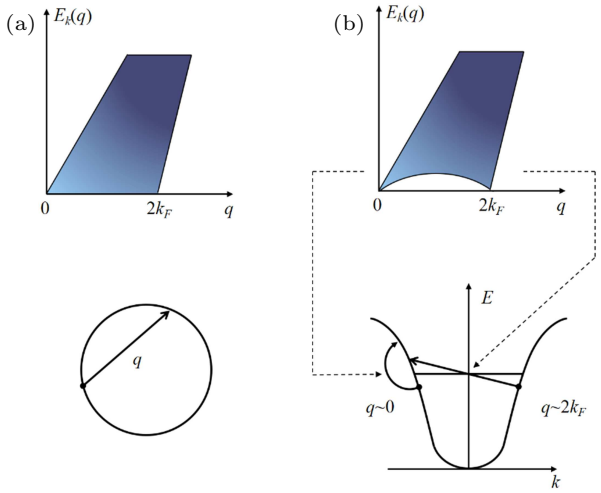


Fig. 1. (a) Particle–hole spectrum for two- or three-dimensional systems. (b) Particle-hole excitation spectrum in one-dimensional systems. Contrary to their higher-dimensional counterparts, one-dimensional systems exhibit particle–hole excitations with well-defined momentum and energy even at small coupling. Low-energy modes appear near $q \sim 0$ and $q \sim 2k_F$. Reproduced with permission from Ref. [1]. Copyright 2004 American Chemical Society.

With the continuous advancement of experimental techniques, high-pressure technology has opened new avenues for exploring the physical properties of solids.[26] Pressure acts as a clean and controllable tuning parameter, playing a crucial role in condensed matter physics by significantly altering structural, electronic, magnetic, and superconducting properties. By modulating interatomic distances, pressure affects hopping integrals, exchange interactions, crystal symmetries, and phase stability, often leading to the emergence of novel quantum states.[27–29] These effects become increasingly pronounced in quasi-one-dimensional systems. As pressure increases, electron–electron interactions are gradually enhanced, and the electronic structure of quasi-1D materials may evolve from 1D to higher-dimensional regimes, accompanied by the appearance of various quantum ordered states that may coexist or compete. In this review, we highlight the pivotal role of pressure in tuning crystal structures and correlated electronic states of quasi-1D systems, focusing on the emergence of novel quantum phases and the underlying physical mechanisms governing their evolution.

2. Structural transitions under high pressure

The intrinsic anisotropy and dimensional confinement of quasi-1D systems render them highly sensitive to external perturbations. In quasi-1D materials, the application of pressure alters atomic arrangements, bond lengths, and bond angles, and can even induce structural phase transitions.[30,31] These pressure-induced structural modifications can lead to significant changes in physical properties, giving rise to novel quantum states and physical phenomena that are absent at ambient pressure.[32,33] Over the past few decades, high-pressure studies have revealed a wide range of novel behaviors in quasi-1D materials, leading to many scientific achievements in the modulation of their structural, electronic, and magnetic properties. One of the most widely studied families is transition metal trichalcogenides MX_3 (M = IVB and VB group; X = S, Se, Te), which possess a typical quasi-1D van der Waals structure. In these compounds, MX_6 trigonal prisms are connected along the b-axis to form quasi-1D chains.[34,35] Due to their strong structural anisotropy, these materials are highly sensitive to external pressure, making pressure an effective tool to tune both orbital and electronic degrees of freedom. For quasi-1D MX_3 compounds (M = Hf, Ti, Zr; X = S, Se, Te), the crystal structures belong to the $P2_1/m$ space group at ambient pressure, and undergo compression to an isostructural phase with a volume collapse of about 5%, accompanied by changes in electronic properties.[33,36,37] As shown in Figs. 2(a) and 2(b), x-ray diffraction (XRD) measurements of HfS_3,[36] reveal a pressure-induced structural transition near 17 GPa, with the high-pressure phase remaining stable up to at least 70.7 GPa. Concurrently, HfS_3 undergoes an insulator to semiconductor transition near 17 GPa. With further compression, superconductivity emerges above 50.6 GPa as HfS_3 enters a semimetallic state. The superconducting transition temperature T_c increases with pressure, reaching 8.1 K at 121 GPa. A similar structural evolution is observed in the pressurized quasi-1D ternary transition-metal chalcogenide $Ta_2Pd_3Te_5$. In this material, increasing pressure reduces interlayer distances

and promotes the formation of covalent bonds between interchain Te atoms, while the lattice symmetry is preserved up to 45 GPa.[38] At the same time, phonon softening is observed, underscoring the key role of electron–phonon coupling in the emergence of superconductivity under high pressure (see Figs. 2(c) and 2(d)).

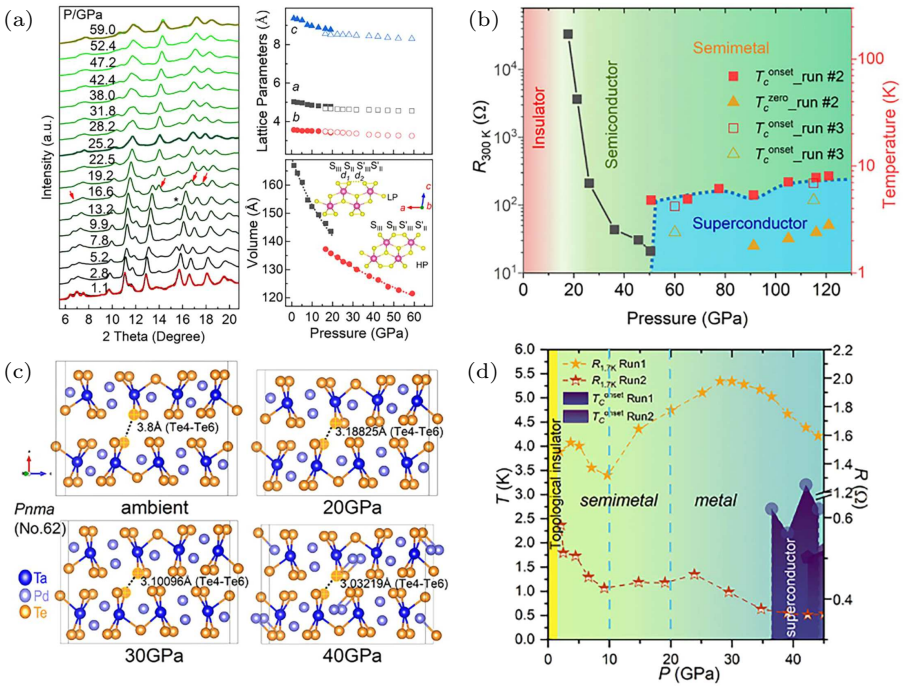


Fig. 2. (a) XRD results of HfS_3 under high pressure. (b) Proposed phase diagram of HfS_3 based on electrical measurements. Reproduced with permission from Ref. [36]. Copyright 2023 American Chemical Society. (c) The crystal structural evolution of $Ta_2Pd_3Te_5$ at various pressures predicted by DFT calculations. (d) Pressure–temperature phase diagram for the entire pressure region, and the right panel shows specific resistance values at 1.7 K as a function of pressure. Reproduced with permission from Ref. [38]. Copyright 2024 American Chemical Society.

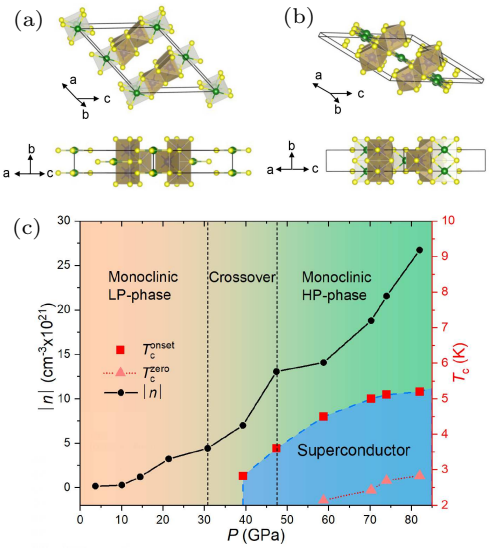


Fig. 3. Schematic representations of (a) the LP phase at 9 GPa and (b) the HP phase at 52 GPa of Ta_2PdS_6 along the *b* axis. (c) Phase diagram under high pressures. The left axis shows the absolute value of the carrier density $[|n| = 1/(|R_H| \cdot e)]$ at 10 K. The right axis corresponds to the onset critical temperature T_c^{onset} and the zero-resistance temperature T_{zero}. Reproduced with permission from Ref. [40]. Copyright 2024 American Physical Society.

In addition, other quasi-1D ternary transition-metal chalcogenides have also been intensively studied under high pressures. For instance, Ta_2PdQ_6 (Q = S, Se) have a monoclinic phase structure ($C2/m$) at ambient pressure,[39] which undergoes an isostructural phase transition from the monoclinic low-pressure (LP) phase to the monoclinic high-pressure (HP) phase, accompanied by the emergence of superconductivity.[40] Due to the weak van der Waals interactions perpendicular to the chain direction, the interlayer distance decreases significantly faster than in the other two crystallographic directions under compression. The structures of the LP-phase and HP-phase are illustrated in Figs. 3(a) and 3(b). Theoretical calculations indicate that the HP-phase has a higher electron state density near the Fermi level. The phase diagram of Ta_2PdS_6 is shown in Fig. 3(c). According to the structural symmetry analysis and electrical transport measurements, the phase diagram can be divided into two distinct regions: the LP-phase region spanning 0 to 30.8 GPa, characterized by an insulator-to-metal transition, and the pressure-induced superconducting HP-phase region above 30.8 GPa. However, for Ta_2PdSe_6, XRD results show that no structural phase transition occurs up to 36.2 GPa, although superconductivity is already present.[41] This suggests that the effect of high pressure on crystal structures is strongly dependent on the anion radius and bonding characteristics, leading to different structural evolution behaviors in isostructural materials under pressure. It is worth noting that continuous structural transformations and substantial changes in physical properties ob-

served under high pressure are challenging to achieve through conventional chemical substitution or external-field regulation techniques.

The tendency for quasi-1D crystal structures to degenerate or become amorphous under high pressure has also been observed. A representative example is the quasi-1D material $(TaSe_4)_2I$, which retains the quasi-1D amorphous chains under high pressure. At ambient pressure, $(TaSe_4)_2I$ has a body-centered tetragonal unit cell (space group $I\bar{4}22$), containing two adjacent chains with four $TaSe_4$ units in each chain and four halogen iodine atoms, as shown in Fig. 4(a).[42,43] By compressing $(TaSe_4)_2I$, Yang's group[43] realized a novel solid-state phase with a combination of long-range order and short-range disorder. With increasing pressure, the lattice of $(TaSe_4)_2I$ gradually contracts. Interestingly, while the interchain distance (d_{inter}) continuously decreases, the intrachain distance (d_{intra}) remains relatively unchanged below approximately 8 GPa (Figs. 4(b) and 4(c)). Correspondingly, as shown in Fig. 4(d), the quasi-1D nature of the system first weakens and then is restored above 8 GPa. The pressure-temperature phase diagram in Fig. 4(e) reveals that high pressure induces amorphization of the $TaSe_4$ atomic chains while preserving the long-range periodicity of the chain lattice, resulting in a novel solid-state phase characterized by short-range disorder and long-range order. Specifically, pressure reduces both the interchain distance and chain diameter, which shows significant contraction above 8 GPa, leading to local structural disorder. This structural transformation triggered a counterintuitive insulator-to-superconductor transition, with superconductivity appearing above approximately 20 GPa. High pressure suppressed the CDW state and enhanced electron pairing interactions, likely through disorder-mediated Coulomb screening, enabling superconductivity in a system with amorphous atomic chains. Similarly, Pei *et al.*[44] reported pressure-induced amorphization and superconductivity in the $(NbSe_4)_2I$. In this case, although amorphization occurs, the quasi-1D Nb–Se chains remain structurally intact, which provides a pathway for superconductivity.

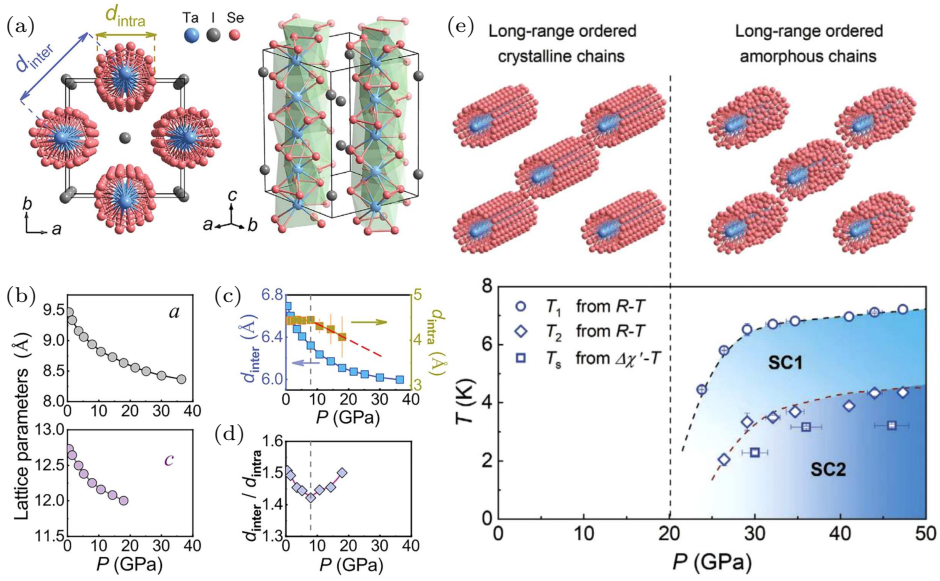


Fig. 4. (a) Schematic crystal structure of $(TaSe_4)_2I$ projected in the a–b plane (left) and along the c-axis (right). (b) Pressure dependence of the lattice parameters a and c. (c) Evolution of the interchain distance d_{inter} and the intrachain diameter d_{intra} with pressure. The red dashed line is a linear fit of d_{intra} above 8 GPa. (d) Pressure-induced changes in the ratio d_{inter}/d_{intra}. (e) Pressure-temperature phase diagram of $(TaSe_4)_2I$. At pressures above $\sim$ 20 GPa, the insulating linear chain compound is transformed into a superconducting quasi-1D system made up of long-range-ordered amorphous atomic chains. Two superconducting regimes are identified: SC1, characterized by intrachain pairing, and SC2, associated with interchain coupling.[43] Reproduced with permission from Ref. [43]. Copyright 2020 John Wiley and Sons.

3. Quantum state evolution under high pressure

3.1. Pressure-tuning of charge density wave and superconductivity

CDW and superconductivity are two distinct electronic states in condensed matter physics. The emergence of CDW necessitates both Fermi surface nesting and electron–phonon coupling, which can lead to a partially gapped Fermi surface, thereby reducing the density of states at the Fermi energy. For a long time, the coexistence and competition between these two phenomena have long been a focal point in quantum materials research, particularly in low-dimensional quantum systems.[45–47] Understanding this relationship not only reveals the microscopic mechanisms of high-temperature superconductivity, but also provides important clues for designing new quantum materials.[48–51] For example, Fig. 5(a) shows the temperature-dependent resistivity of CuTe under pressures up to 13.8 GPa, where CDW-related anomalies are gradually suppressed and reemerge with increasing pressure. The corresponding $d\rho/dT$ curves in Fig. 5(b) reveal an evolution of the CDW transition from a dip to a peak near 8.1 GPa, indicating a pressure-induced reconstruction of CDW order. The phase

diagram of CuTe under high pressure is shown in Fig. 5(c).[52] Under pressure, the pristine CDW1 phase transforms into the CDW2 phase at 6.5 GPa. First-principles calculations indicate that CDW1 is driven by nesting effects, whereas CDW2 likely arises from electronic correlation interactions. Strikingly, pressure-induced superconductivity emerges, exhibiting a dome-shaped phase diagram. The superconducting transition is significantly broadened across the CDW1–CDW2 crossover, suggesting a complex interaction between the two CDW states and superconductivity. These pressure-tuned phenomena provide new insights into the intrinsic properties and phase transition mechanisms of correlated low-dimensional systems, as well as effective strategies for the rational design of novel functional materials.

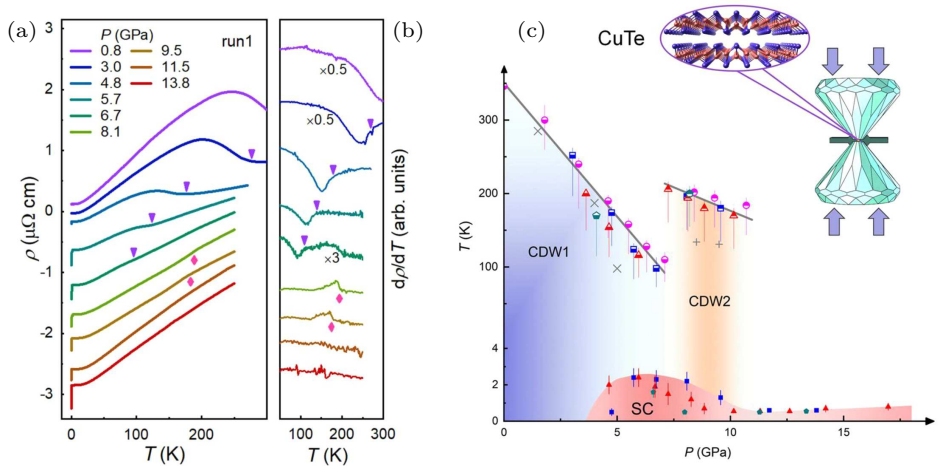


Fig. 5. (a) Resistivity (ρ) and (b) its temperature derivative $\mathrm{d}\rho/\mathrm{d}T$ for CuTe in the pressure range 0.8–13.8 GPa. The onset transition temperatures of anomalies with hump-like and kink-like features are marked by purple triangles and pink rhombuses, respectively; all curves are vertically offset for clarity. (c) Temperature-pressure phase diagram of CuTe single crystal, showing the pressure dependences of the CDW transition temperatures T_{CDW1} and T_{CDW2}, and the superconducting transition temperature $T_{\mathrm{c}}^{\mathrm{onset}}$. Reproduced with permission from Ref. [52]. Copyright 2023 Elsevier.

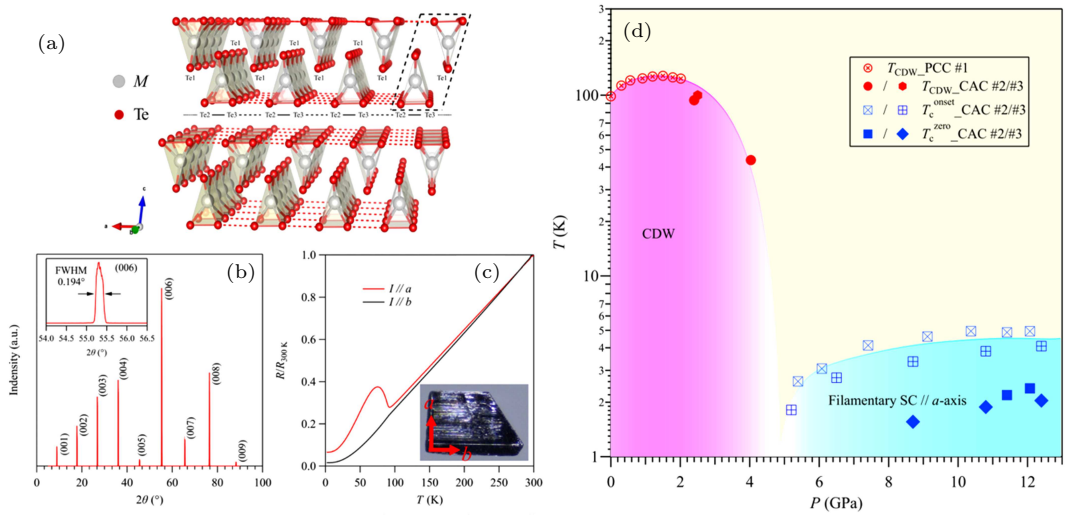


Fig. 6. (a) Crystal structure of $M\mathrm{Te}_3$ (M = Zr, Hf). (b) X-ray diffraction pattern of the single-crystal HfTe_3 showing only the (00l) diffraction peaks. The inset shows the FWHM of the (006) Bragg peak. (c) Temperature dependence of the normalized resistance along the a- and b-axes, $R(T)/R_{300\ \mathrm{K}}$, measured on the same piece of sample at ambient pressure. The inset displays a photo of the crystal showing fringes extending along the b-axis. (d) Temperature-pressure phase diagram of HfTe_3 single crystal. The CDW transition temperature T_{CDW} and the superconducting transition temperatures $T_{\mathrm{c}}^{\mathrm{onset}}$ and $T_{\mathrm{c}}^{\mathrm{zero}}$ are determined from resistance measurements along the a-axis. Reproduced with permission from Ref. [53]. Copyright 2021 Springer Nature.

A recent study by Liu *et al.*[53] on the transition metal trichalcogenide HfTe_3 reported that single crystals exhibit a CDW transition at higher $T_{\mathrm{CDW}} \sim 93$ K, but show no signs of superconductivity down to 50 mK at ambient pressure (see Figs. 6(a)–6(c)). High-pressure experiments revealed that the CDW state can be completely suppressed at 5 GPa. Under these conditions, superconductivity emerges in the a-axis resistance at $T \sim 4$–5 K, while the resistance along the b- and c-axes exhibits a drop at $T \sim 1.5$ K without clear evidence of bulk superconductivity. The temperature–pressure phase diagram of HfTe_3, shown in Fig. 6(d), highlights the delicate competition between CDW and superconductivity in this quasi-1D system. Similar pressure-induced suppression of CDW and emergence of superconductivity have also

been observed in other metallic quasi-1D compounds, including $NbSe_3$,[54,55] TaS_3,[56] and $ZrTe_3$.[57,58] In particular, the CDW state in $NbSe_3$ is influenced by enhanced interchain coupling under pressure, leading to modifications of the CDW modulation wave vectors. This is accompanied by anomalous resistance behavior, suggesting a significant influence of quantum fluctuations on the ground state.[55]

Within the MX_3 family, $TaSe_3$ has been proposed as a quasi-1D topological insulator with a superconducting transition temperature $T_c \sim 2.3$ K, which is gradually suppressed under pressure.[23,59,60] Recent studies have shown that applying high pressure significantly enhances the CDW instability in $TaSe_3$, with the transition temperature shifting to higher values as pressure increases, as shown in Fig. 7.[61] Despite the pronounced enhancement of the CDW transition under pressure, no superconductivity was observed down to 2 K within the studied pressure range. This suggests that superconductivity in $TaSe_3$ is fragile and may be easily suppressed by external perturbations in this quasi-1D system. The low-temperature transport properties remain largely unchanged under pressure, consistent with the observed giant and anisotropic planar Hall effect,[62] which is attributed to the anisotropic scattering of Dirac fermions. This behavior suggests a correlation between low-temperature transport and the topological band structure. Furthermore, the pressure-induced CDW transition has negligible impact on the topological nature of the electronic states, providing a promising platform for realizing novel pressure-stabilized topological phases. High-pressure Raman spectroscopy offers additional insight into the lattice dynamics, revealing lattice hardening and a kink in the in-plane mode frequency around 6 GPa. These observations provide further evidence for the occurrence of a CDW-like phase transition and potential topological phase transitions.

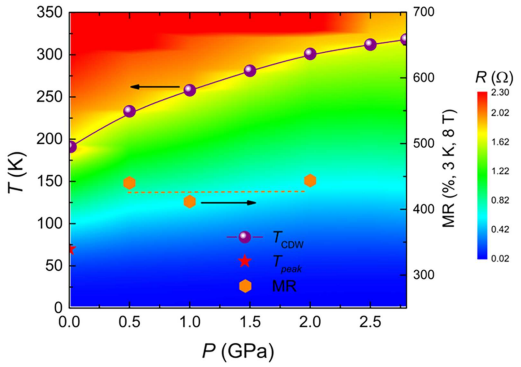


Fig. 7. Hydrostatic pressure-temperature phase diagram of $TaSe_3$. Color represents the evolution of resistance as a function of temperature and pressure. MR denotes the magnetoresistance measured at 3 K and 8 T. Reproduced with permission from Ref. [61]. Copyright 2024 American Physical Society.

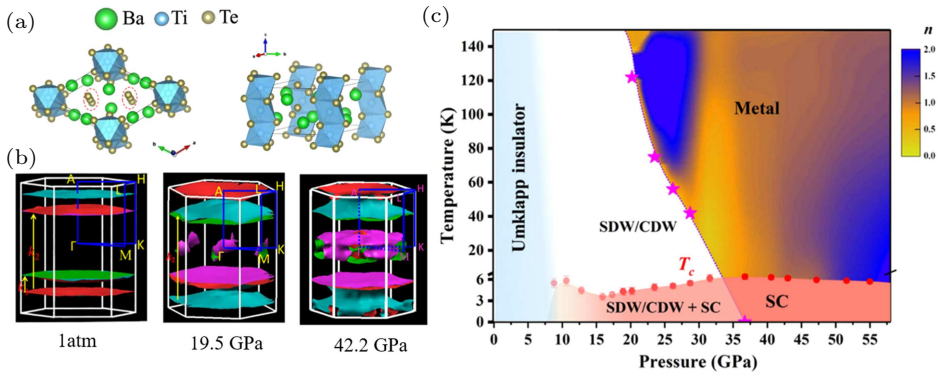


Fig. 8. (a) Schematic plots of the Ba_3TiTe_5 crystal structure, projected along and perpendicular to the c axis, respectively. The atoms enclosed by red dashed circles represent Te chains at the Te(2) site. (b) Calculated Fermi surfaces at ambient pressure, 19.5 GPa, and 42.2 GPa, respectively. (c) Pressure-temperature phase diagram of Ba_3TiTe_5. The red circle denotes the superconducting temperature T_c, and the purple star is the metallic–semiconducting crossover temperature T_m. In the metallic region, the color shading represents the value of the exponent $n = d(\ln(R - R_0))/d(\ln(T))$. Reproduced with permission from Ref. [63]. Copyright 2019 Springer Nature.

Some metastable quasi-1D materials can be synthesized under high pressure. Zhang *et al.*[63] synthesized Ba_3TiTe_5 under high-pressure, high-temperature (HPHT) conditions. In this compound, the crystal structure consists of infinite octahedral $TiTe_6$ chains (Fig. 8(a)), with the conducting paths along the $TiTe_6$ and Te chains, which are separated by Ba cations and thus exhibiting quasi-1D conducting characteristics. Under high pressure, the interchain distance decreases by 12.1%, enhancing Fermi surface nesting and triggering SDW or CDW instabilities, leading to gap formation and a pressure-induced metal–semiconductor crossover (Fig. 8(b)). The temperature-pressure phase diagram of Ba_3TiTe_5 is shown in Fig. 8(c). As the SDW/CDW orders are fully suppressed, the superconducting transition temperature T_c reaches a maximum of 6 K, accompanied by non-Fermi liquid behavior, indicating a close relationship between the enhancement of superconductivity and CDW/SDW fluctuations.

3.2. Topological phase transition and superconductivity under pressure

Furthermore, high pressure is a powerful tool for inducing superconductivity and driving topological quantum phase transitions in quasi-1D topological Bi-based materials. As shown in Fig. 9(a), superconductivity emerges in β-Bi_4I_4 at 17.6 GPa,

with T_c peaking at 6 K at 23 GPa, followed by a gradual suppression at higher pressures, exhibiting a typical dome-like evolution.[64] Density functional theory (DFT) calculations reveal multiple pressure-driven topological transitions: at ambient pressure, β-Bi_4I_4 is a strong topological insulator (STI) with band inversion at the Y point. As pressure increases, the conduction band minimum (CBM) and valence band maximum (VBM) converge at the M point, closing the band gap. Upon reopening, the system transitions into a weak topological insulator (WTI). With further pressure, band inversion at the Y point restores the STI phase (see Fig. 9(b)). These calculated transitions are consistent with experimental resistivity trends, highlighting the intricate interplay between topological order and superconductivity under high pressure. A similar phenomenon is observed in α-Bi_4Br_4,[65] where superconductivity first appears at 3.8 GPa with a zero-resistance temperature $T_c^{zero} \sim 6.8$ K, and gradually vanishes above 12 GPa. Notably, the superconducting phase may coexist with a nontrivial topological state within a narrow pressure range between 3.8 GPa and 4.3 GPa. Zhou *et al.*[66] have performed a high-pressure study on $Bi_4(I_{1-x}Br_x)_4$ crystals grown by two different methods. Remarkably, crystals grown by the chemical vapor transport (CVT) method and the self-flux method show clearly different pressure effects, as shown in Figs. 9(c)–9(f). Compared to the β-Bi_4I_4, the critical pressure for the observation of superconductivity and the optimal pressure for the highest T_c are both slightly enhanced. In addition, the recently discovered quasi-1D compound $Bi_{19}S_{27}I_3$ undergoes a pressure-induced semiconductor-to-metal transition below 11.5 GPa, during which a density-wave-like transition emerges. At higher pressures, the low-temperature resistivity exhibits an upturn, attributed to enhanced electron scattering arising from Anderson-type weak localization. These behaviors indicate that high pressure induces changes in the electronic structure.[67] Collectively, these studies provide valuable insights into pressure-induced superconductivity, topological quantum phases, and density-wave phenomena in Bi-based quasi-1D materials.

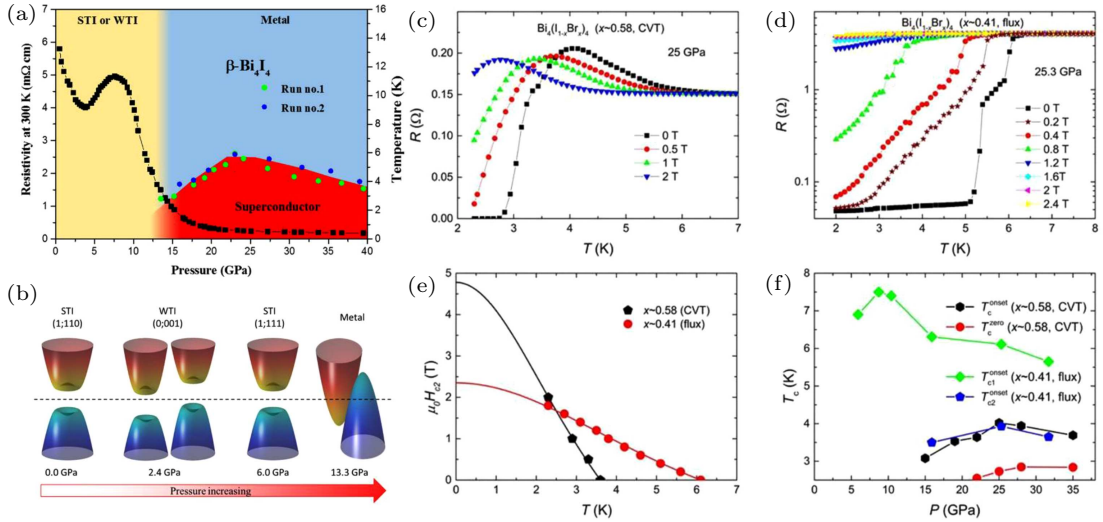


Fig. 9. (a) Superconducting transition temperature T_c as a function of pressure for β-Bi_4I_4. The green and blue circles represent T_c values extracted from different resistivity measurements. (b) Schematic illustrations of the band structure evolution under various pressures. In the STI phase, band inversion occurs at one of the time-reversal-invariant momentum (TRIM) points in the Brillouin zone, whereas in the WTI phase, band inversion occurs at two TRIM points. In the metallic phase, the Fermi level crosses the bands.[64] Reproduced with permission from Ref. [64]. Copyright 2018 Springer Nature. (c), (d) Superconducting transitions of $Bi_4(I_{1-x}Br_x)_4$ measured under different magnetic fields for the $x \sim 0.58$ (CVT) and $x \sim 0.41$ (flux) crystals. (e) Temperature dependence of $\mu_0 H_{c2}$. The solid lines are fits based on the Ginzburg–Landau formula. (f) Pressure dependence of T_c. T_c^{onset} and T_c^{zero} represent the onset critical temperature and zero-resistance critical temperature of superconductivity, respectively. Reproduced with permission from Ref. [66]. Copyright 2023 IOP Publishing.

3.3. Superconductivity and magnetic quantum critical point

One of the most remarkable universal characteristics of high-temperature superconductors is that the superconducting phase emerges in the vicinity of the AFM phase, and clarifying the interplay of competition and coexistence between these two phases is an important and long-standing challenge.[68] In high T_c cuprates and iron-based superconductors, the emergence of unconventional superconductivity is often closely related to magnetic ordering. By carrier doping or pressure tuning, the antiferromagnetic order can be gradually suppressed, and then the superconducting phase emerges.[69–72] Compared to layered superconductors, unconventional superconductivity in quasi-1D materials has received relatively less attention, and high pressure is one of the important methods for tuning. The atomic electron configuration and exchange interaction can be regulated by pressure, leading to magnetic phase transitions, exploring and realizing magnetic quantum critical points, and discovering possible unconventional superconductivity.

The quasi-1D spin-ladder compound $BaFe_2S_3$, which can have superconductivity induced by high pressure,[73,74] opens

new avenues for exploring iron-based quasi-1D materials. The crystal structures of $BaFe_2S_3$ and $BaFe_2Se_3$ feature quasi-1D Fe_2X_3 (X = S and Se) ladders formed by edge-shared FeX_4 tetrahedra (see Fig. 10(a)). $BaFe_2S_3$ exhibits a stripe-type AFM ordering (see Figs. 10(b) and 10(c)), while $BaFe_2Se_3$ has a block-type AFM structure.[16,17,75,76] As shown in the pressure-temperature phase diagram of $BaFe_2S_3$ (Fig. 10(d)), the antiferromagnetic insulating state at ambient pressure is transformed into a metallic state at $P_c \sim 10$ GPa, and the optimum $T_c = 24$ K emerges above P_c.[74] Powder neutron diffraction and μSR measurements show that the stripe-type AFM ordering temperature increases up to 2.6 GPa without significant change in the magnetic moment. Theoretical calculations indicate that the magnetism is highly sensitive to the Fe-S bond lengths and bond angles under pressure.[77] Similar pressure-induced superconductivity is observed in $BaFe_2Se_3$.[78] As shown in Fig. 10(f), the slope of local magnetic moment versus pressure shows an anomaly across the insulator–metal transition pressure. The local magnetic moment continuously decreases with increasing pressure, and superconductivity emerges only when the local magnetic moment value is comparable to that in the iron-pnictide superconductors. This correlation indicates a close connection between the suppression of local magnetism and the emergence of superconductivity in these quasi-1D ladder compounds.

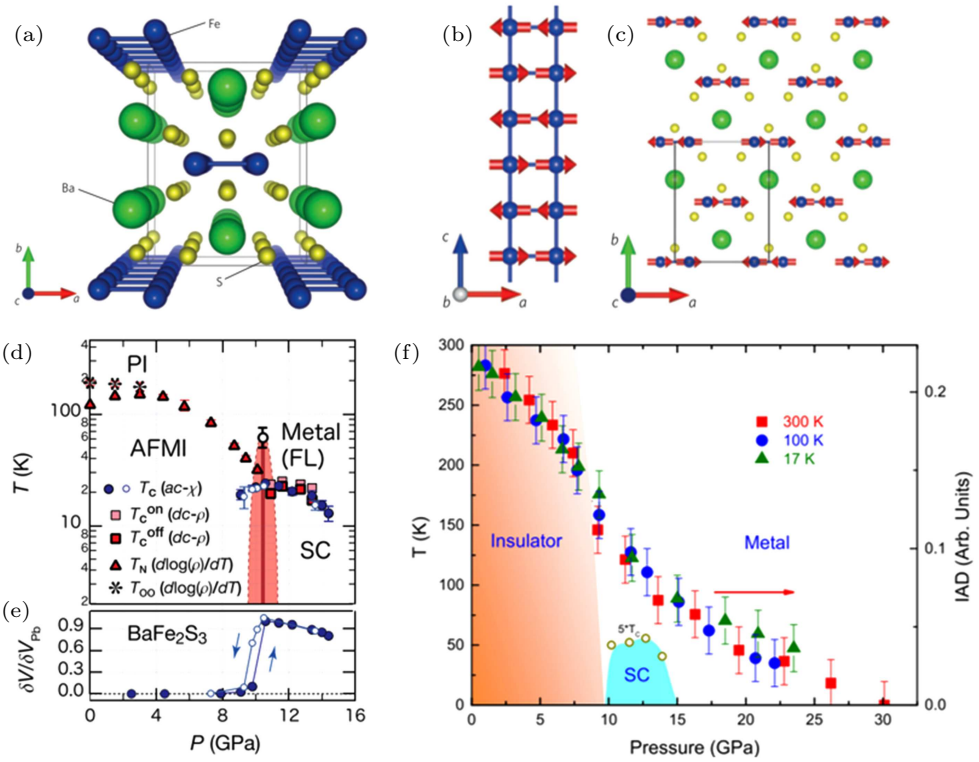


Fig. 10. (a) Crystal structure of $BaFe_2S_3$. (b) Magnetic structure within the ladder: magnetic moments aligned along the a-axis form ferromagnetic units along the rung direction, and are stacked antiferromagnetically along the leg direction. (c) View of the magnetic structure along the c-axis: inter-ladder coupling of Fe spins is ferromagnetic along the (110) direction and antiferromagnetic along the $(1\bar{1}0)$ direction. Reproduced with permission from Ref. [73]. Copyright 2015 Springer Nature. (d) Pressure–temperature phase diagram of $BaFe_2S_3$ constructed from both dc resistivity (red) and ac susceptibility (blue) measurements. (e) Pressure dependence of the superconducting volume fraction at ~ 4 K derived from the ac susceptibility measurements; filled (open) symbols represent increasing (decreasing) pressure processes. Reproduced with permission from Ref. [74]. Copyright 2015 American Physical Society. (f) Pressure–temperature phase diagram of $BaFe_2Se_3$. The deduced integrated absolute difference (IAD), which is proportional to the Fe local moment, is shown as red squares (300 K), blue circles (100 K), and green triangles (17 K). A slope anomaly in the magnetic moment vs pressure indicates an insulator-metal transition. Reproduced with permission from Ref. [78]. Copyright 2017 American Physical Society.

In $BaFe_2(S_{1-x}Se_x)_3$, the magnetic ground state shifts from stripe-type to block-type AFM order at $x = 0.23$, with T_N decreasing from 119 K to 82 K for $x \leq 0.23$, and then slightly increasing for $x \geq 0.23$. This magnetic transition is associated with a structural phase change and the emergence of spin-glass behavior at low temperatures for $x \geq 0.29$.[79–81] The doping-dependent phase diagrams for T_N and the spin glass state temperature T_g are shown in Fig. 11(a).[82] Within the stripe-type AFM structure, T_N is gradually suppressed with increasing Se doping level, while T_N shows gentle enhancements as x increases for the block-type AFM structure. Concurrently, T_g shows a nearly dome-like doping-dependent phase diagram within the block-type AFM phase. Figures 11(b)–11(d) display the high-pressure resistance curves of $BaFe_2(S_{1-x}Se_x)_3$ samples. Compared with the parent compound $BaFe_2S_3$, higher pressures are required to fully metallize the Se-doped samples. For the sample with $x = 0.07$, a downturn in the resistance curve is observed around 11 K at 8.6 GPa, as indicated by the red arrow. Similar resistance anomalies have also been reported in $BaFe_2Se_3$ and $BaFe_2(S_{0.75}Se_{0.25})_3$ under

comparable pressures and have been attributed to the onset of superconductivity.[83] However, for samples with $x = 0.18$ and $x = 0.37$, pressures over 20 GPa have been applied, but no superconductivity was observed, suggesting that the emergence of superconductivity may be hindered by a complex interplay between AFM order and superconducting pairing. Additionally, the pressure-resistance curves of $BaFe_2(S_{1-x}Se_x)_3$ show an electronic phase transition near 18 GPa (Fig. 11(e)). The resistance initially decreases and then increases, which may be associated with a first-order structural transition similar to that observed in $BaFe_2S_3$. This transition is characterized by significant b-axis shortening, and resembles the predicted magnetic shift from block- to stripe-type AFM at 12 GPa, suggesting that the electronic and magnetic transitions are coupled in this quasi-1D system.[84]

In addition to the quasi-1D Fe-based superconductors, high pressure also plays a crucial role in tuning quasi-1D Cr- and Mn-based materials. The $A_2Cr_3As_3$ (A = K, Rb, Cs) family represents the first Cr-based superconductors with a quasi-1D crystal structure at ambient pressure. In these compounds, the $(Cr_3As_3)^{2-}$ units form double-walled subnanotubes, consisting of face-sharing $Cr_{6/2}(As_{6/2})$ octahedral linear chains in the inner and outer walls, respectively (see Figs. 12(a)–12(d)).[85–87] The superconducting transition

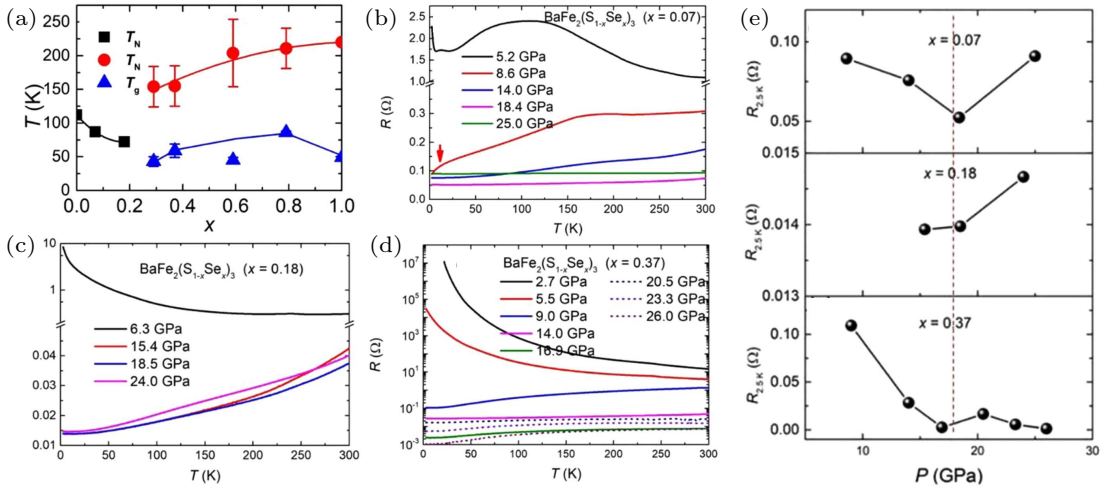


Fig. 11. (a) Doping-dependent phase diagram of $BaFe_2(S_{1-x}Se_x)_3$ showing the antiferromagnetic (AFM) transition temperature T_N and the spin-glass temperature T_g. (b), (c) Temperature-dependent resistance under pressure for two lightly Se-doped samples exhibiting stripe-type AFM order. (d) Temperature-dependent resistance for a Se-doped sample with block-type AFM order. (e) Pressure dependence of resistance at 2.5 K for three Se-doped samples. A resistance dip appears around 18 GPa for all three samples, indicating the occurrence of an electronic phase transition. Reproduced with permission from Ref. [82]. Copyright 2022 IOP Publishing.

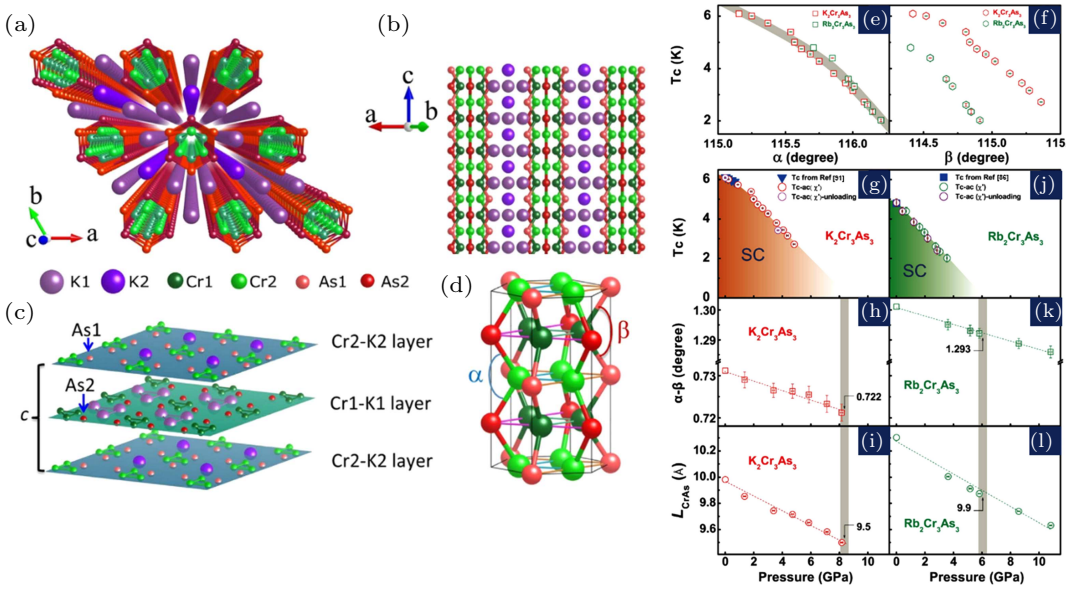


Fig. 12. (a) Crystal structure of $K_2Cr_3As_3$, featuring double-walled subnanotubes formed by Cr and As atoms. (b) Views of the lattice structure parallel to the *ac* plane. (c) Alternative distribution of K1 and K2 ions between layers. (d) Sketch of the two different bond angles in CrAs chains. (e), (f) α and β angles versus T_c for $A_2Cr_3As_3$ (A = K and Rb) superconductors. (g)–(i) Pressure dependences of T_c, α–β, and L_{CrAs} for $K_2Cr_3As_3$ superconductor. (j)–(l) T_c, α–β, and L_{CrAs} as functions of pressure for $Rb_2Cr_3As_3$ superconductor. The solid triangles in (g) are data taken from Ref. [91]. The open circles in (g), (j) represent T_c obtained from our $A_2Cr_3As_3$ samples upon loading and unloading, respectively. The solid squares in (j) are data taken from Ref. [86]. (h), (k) Pressure dependence of the α–β angle for the samples investigated. (i), (l) Distance between CrAs chains (L_{CrAs}) as a function of pressure for $K_2Cr_3As_3$ and $Rb_2Cr_3As_3$, respectively. [89] Reproduced with permission from Ref. [89]. Copyright 2016 Springer Nature.

temperatures (T_c) of $K_2Cr_3As_3$, $Rb_2Cr_3As_3$, and $Cs_2Cr_3As_3$ are 6.1 K, 4.8 K, and 2.2 K, respectively. Under physical pressure, both $K_2Cr_3As_3$ and $Rb_2Cr_3As_3$[88–90] exhibit reductions in interchain spacing as well as compression within the $[Cr_3As_3]_\infty$ chains. These structural changes lead to a gradual weakening of electronic correlations and magnetic instability. Consequently, both T_c and the upper critical field ($\mu_0 H_{c2}$) of these compounds are significantly suppressed, eventually falling below the Pauli paramagnetic limit, as shown in Figs. 12(e)–12(l). This behavior suggests a possible transition of the pairing mechanism from spin-triplet to spin-singlet.[88,89]

In contrast, the removal of one alkali ion from the parent compounds yields ACr_3As_3 ($A = K, Rb$), which retain similar quasi-1D structures but experience effective chemical pressure due to unit cell contraction. The T_c of KCr_3As_3 and $RbCr_3As_3$ reach approximately 5 K and 7.3 K, respectively, with $\mu_0 H_{c2}$ significantly exceeding the Pauli limit. Cao's group[92,93] proposed, based on combined experimental and theoretical studies, that the superconductivity is closely related to the intercalation of H^+ ions into the $[Cr_3As_3]_\infty$ chains. By comparing the effects of physical and chemical pressure, Liu *et al.*[90] concluded that the highest T_c in quasi-1D Cr-based superconductors occurs when both interchain and intrachain distances of the $[Cr_3As_3]_\infty$ chains reach optimal values, specifically $a \sim 9.2$ Å and $c \sim 4.21$ Å. This finding underscores the critical role of both interchain and intrachain distances in governing superconductivity in these systems.

In the family of quasi-1D Mn-based compounds AMn_6Bi_5 (A = Na, K, Rb, and Cs), pressure-induced unconventional superconductivity exhibits a complex interplay with magnetism. The crystal structure of KMn_6Bi_5 consists of infinite $[Mn_6Bi_5]^-$ columns aligned along the b axis, with K^+ cations located between the columns. Magnetic susceptibility measurements reveal one-dimensional characteristics with an antiferromagnetic transition at approximately 75 K (see Fig. 13(b)). Density functional theory (DFT) calculations predict helical magnetic order for $RbMn_6Bi_5$ (see Fig. 13(c)). The AMn_6Bi_5 family (A = K, Rb, Cs) exhibits long-range AFM order at ambient pressure. Upon applying pressure, localized electrons become itinerant, suppressing the AFM order and inducing superconductivity near the magnetic quantum critical point (Figs. 13(d) and 13(e)). With further pressure increase, a superconducting dome forms, with the maximum T_c values of approximately 9.3 K, 9.5 K, and 9.6 K for KMn_6Bi_5, $RbMn_6Bi_5$, and $CsMn_6Bi_5$, respectively.[19,94–97] The upper critical fields $\mu_0 H_{c2}$ of these materials all exceed the Pauli limit, indicating an unconventional pairing mechanism. Interestingly, alkali metal substitution has minimal effect on both the critical pressure required for superconductivity onset and the maximum T_c, suggesting that the AFM-to-superconducting transition in the AMn_6Bi_5 family is intimately linked to the quasi-1D $[Mn_6Bi_5]^-$ chains. DFT calculations further reveal that near the critical

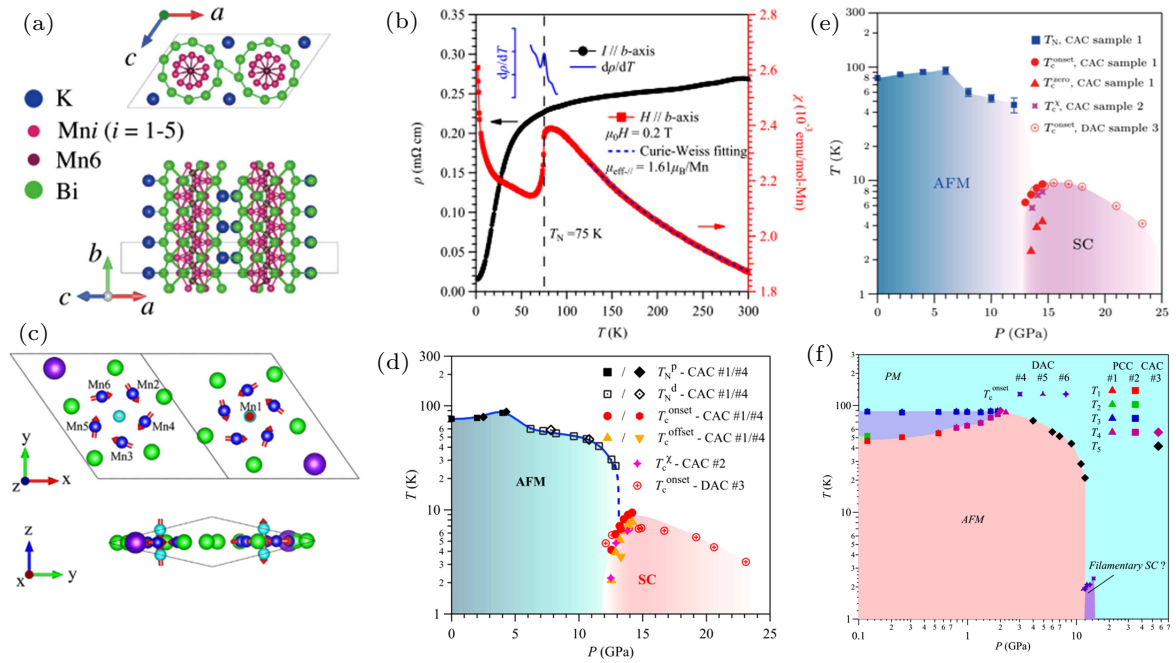


Fig. 13. (a) Crystal structure of KMn_6Bi_5 viewed along the b axis (top) and perpendicular to the b axis (bottom). (b) Temperature-dependent resistivity of KMn_6Bi_5 single crystal with current applied parallel and perpendicular to the b axis. Reproduced with permission from Ref. [94]. Copyright 2022 American Physical Society. (c) Schematic of the helical antiferromagnetic configuration in $RbMn_6Bi_5$ predicted by DFT calculations. Reproduced with permission from Ref. [19]. Copyright 2021 American Chemical Society. (d) Pressure–temperature phase diagram for KMn_6Bi_5. Reproduced with permission from Ref. [94]. Copyright 2022 American Physical Society. (e) Pressure–temperature phase diagram of $RbMn_6Bi_5$.[95] Reproduced with permission from Ref. [95]. Copyright 2022 IOP Publishing. (f) Pressure–temperature phase diagram of $NaMn_6Bi_5$. T_c^{onset} denotes the possible filamentary superconductivity. Reproduced with permission from Ref. [97]. Copyright 2023 American Physical Society.

pressure, the partial density of states (PDOS) of the Mn $3d_{yz}$ orbital near the Fermi level increases anomalously, while those of the d_{xz} and d_{z^2} orbitals decrease abnormally. This indicates that the transition from AFM order to superconductivity is accompanied by an orbital-selective process involving Mn 3d electrons.

In contrast to the AMn$_6$Bi$_5$ compounds, NaMn$_6$Bi$_5$ exhibits more intricate magnetic behavior. It undergoes three successive magnetic transitions upon cooling, occurring at approximately 87 K (T_3), 53 K (T_2), and 47 K (T_1), respectively, with the two lower-temperature transitions identified as antiferromagnetic in nature. The nature of the highest-temperature transition T_3 remains unclear. Compared with its sister compounds, NaMn$_6$Bi$_5$ also displays non-Fermi liquid behavior and a significantly enhanced Sommerfeld coefficient at low temperatures, indicative of strong electronic correlations. Recent high-pressure studies by Cheng's group[97] reveal that NaMn$_6$Bi$_5$ does not exhibit bulk superconductivity up to 69 GPa, although a slight resistance drop is observed in a narrow pressure window between 12 GPa and 14.4 GPa. The evolution of the magnetic transitions under pressure is complex: the intermediate phase between T_1 and T_2 rapidly disappears, with T_2 vanishing below 0.25 GPa. Meanwhile, T_1 shifts to higher temperatures but becomes indistinct above 0.79 GPa, where a new transition, T_4, emerges. The temperature of T_4 increases with pressure and eventually merges with the nearly pressure-independent T_3 near 2 GPa. At 4 GPa, T_4 disappears, giving way to another transition T_5, which then shifts to lower temperatures and vanishes around 13 GPa, marking the complete suppression of antiferromagnetic order. These multiple magnetic transitions are likely related to the small size of the Na ions, which enhance magnetic frustration in the system. Overall, high-pressure studies of quasi-1D Mn-based materials such as NaMn$_6$Bi$_5$ have deepened the understanding of the interplay between antiferromagnetism and superconductivity in quasi-1D systems dominated by 3d electrons.[98]

4. Summary and prospects

High-pressure studies of quasi-1D materials have uncovered deep connections between dimensionality, electron configurations, and quantum states, providing a unique perspective for tuning and understanding competing orders in strongly correlated systems. Pressure reduces interatomic distances, leading to the enhancement of orbital overlap, which in turn increases bandwidth and suppresses electronic localization. Additionally, pressure alters the exchange interactions, affecting the degree of magnetic frustration. By continuously tuning external pressure, one can stabilize exotic quantum phases, explore quantum phase transitions and novel emergent phenomena. Simultaneously, certain critical challenges remain unexplored due to technical limitations. It is still to be determined whether these pressurized superconductors can still be categorized as 'quasi-1D', and if so, what dimensionality their superconducting gap would exhibit. High-pressure cells capable of measuring the anisotropic transport and thermal properties of quasi-1D crystals under strong magnetic fields, particularly under hydrostatic conditions, are essential to understand the superconducting gap symmetry and reveal the mechanism of unconventional superconductors. Additionally, pressure techniques that enable the measurement of superconducting tunneling spectra in quasi-1D materials would be valuable. Future research should integrate ultra-high-pressure (hydrostatic conditions) experimental techniques, nanoscale *in situ* characterization, anisotropic transport measurements, and machine learning-assisted electronic structure calculations together to explore the potential emergence of exotic states, such as quasi-1D superconductivity and topological superconductivity under extreme conditions.

Acknowledgements

Project supported by the National Natural Science Foundation of China (Grant Nos. U1932217, 12374135, and 12304193), the National Key R&D Program of China (Grant Nos. 2024YFA1408400 and 2018YFA0704300), the Strategic Priority Research Program (B) of the Chinese Academy of Sciences (Grant No. XDB25000000), the Southeast University Interdisciplinary Research Program for Young Scholars, and the Open Research Fund of the Key Laboratory of Quantum Materials and Devices (Southeast University), Ministry of Education, China.

References

[1] Giamarchi T 2004 *Chem. Rev.* **104** 5037
[2] Haldane F D M 1981 *J. Phys. C: Solid State Phys.* **14** 2585
[3] Shchegolev I F 1972 *Phys. Status Solidi A* **12** 9
[4] Zhang W and Sá De Melo C A R 2007 *Adv. Phys.* **56** 545
[5] Denholme S J, Yukawa A, Tsumura K, Nagao M, Tamura R, Watauchi S, Tanaka I, Takayanagi H and Miyakawa N 2017 *Sci. Rep.* **7** 45217
[6] Gooth J, Bradlyn B, Honnali S, Schindler C, Kumar N, Noky J, Qi Y, Shekhar C, Sun Y, Wang Z, Bernevig B A and Felser C 2019 *Nature* **575** 315
[7] Boswell F W, Prodan A and Brandon J K 1983 *J. Phys. C: Solid State Phys.* **16** 1067
[8] Autès G, Isaeva A, Moreschini L, Johannsen J C, Pisoni A, Mori R, Zhang W, Filatova T G, Kuznetsov A N, Forro L, Van den Broek W, Kim Y, Kim K S, Lanzara A, Denlinger J D, Rotenberg E, Bostwick A, Grioni M and Yazyev O V 2016 *Nat. Mater.* **15** 154
[9] Ma N, Wang D Y, Huang B R, Li K Y, Song J P, Liu J Z, Mei H P, Ye M and Li A 2023 *Chin. Phys. B* **32** 056801
[10] van Smaalen S 2005 *Acta Crystallogr. A* **61** 51
[11] Hor Y S, Xiao Z L, Welp U, Ito Y, Mitchell J F, Cook R E, Kwok W K and Crabtree G W 2005 *Nano Lett.* **5** 397
[12] Montambaux G 1988 *Phys. Rev. B* **38** 4788
[13] Shaginyan V R, Msezane A Z, Japaridze G S, Artamonov S A and Leevik Y S 2022 *Materials* **15** 3901
[14] Izyumov Y A 1988 *Sov. Phys. Usp.* **31** 689
[15] Hong H Y and Steinfink H 1972 *J. Solid State Chem.* **5** 93
[16] Wang M, Jin S J, Yi M, Song Y, Jiang H C, Zhang W L, Sun H L, Luo H Q, Christianson A D, Bourret-Courchesne E, Lee D H, Yao D X and Birgeneau R J 2017 *Phys. Rev. B* **95** 060502(R)

[17] Nambu Y, Ohgushi K, Suzuki S, Du F, Avdeev M, Uwatoko Y, Munakata K, Fukazawa H, Chi S X, Ueda Y and Sato T J 2012 *Phys. Rev. B* **85** 064413

[18] Bao J K, Tang Z T, Jung H J, Liu J Y, Liu Y, Li L, Li Y K, Xu Z A, Feng C M, Chen H J, Chung D Y, Dravid V P, Cao G H and Kanatzidis M G 2018 *J. Am. Chem. Soc.* **140** 4391

[19] Chen L, Zhao L L, Qiu X L, Zhang Q H, Liu K, Lin Q S and Wang G 2021 *Inorg. Chem.* **60** 12941

[20] Zhou Y, Chen L, Wang G, Wang Y X, Wang Z C, Chai C C, Guo Z N, Hu J P and Chen X L 2022 *Chin. Phys. Lett.* **39** 047401

[21] Sigrist M and Ueda K 1991 *Rev. Mod. Phys.* **63** 239

[22] Xu C Q, Liu Y, Cai P G, Li B, Jiao W H, Li Y L, Zhang J Y, Zhou W, Qian B, Jiang X F, Shi Z X, Sankar R, Zhang J L, Yang F, Zhu Z W, Biswas P, Qian D, Ke X L and Xu X F 2020 *J. Phys. Chem. Lett.* **11** 7782

[23] Lin C, Ochi M, Noguchi R, *et al*. 2021 *Nat. Mater.* **20** 1093

[24] Ma J Z, Nie S M, Gui X, *et al*. 2022 *Nat. Mater.* **21** 423

[25] Ning W, Yu H Y, Liu Y Q, Han Y Y, Wang N, Yang J Y, Du H F, Zhang C J, Mao Z Q, Liu Y, Tian M L and Zhang Y H 2015 *Nano Lett.* **15** 869

[26] Mao H K, Chen X J, Ding Y, Li B and Wang L 2018 *Rev. Mod. Phys.* **90** 015007

[27] Sun J P, Matsuura K, Ye G Z, Mizukami Y, Shimozawa M, Matsubayashi K, Yamashita M, Watashige T, Kasahara S, Matsuda Y, Yan J Q, Sales B C, Uwatoko Y, Cheng J G and Shibauchi T 2016 *Nat. Commun.* **7** 12146

[28] Rose E, Loose C, Kortus J, Pashkin A, Kuntscher C A, Ebbinghaus S G, Hanfland M, Lissner F, Schleid T and Dressel M 2013 *J. Phys. Condens. Matter* **25** 014006

[29] Itoi M, Nakamura T and Uwatoko Y 2022 *Materials* **15** 4638

[30] Clarke S M, Powderly K M, Walsh J P S, Yu T, Wang Y B, Meng Y, Jacobsen S D and Freedman D E 2019 *Chem. Mater.* **31** 955

[31] Li Y H, Zhou P, Ding C, Lu Q, Wang X M and Sun J 2024 *Chin. Phys. B* **33** 106102

[32] Abdel-Hafiez M, Shi L F, Cheng J G, Gorlova I G, Zybtsev S G, Pokrovskii V Y, Ao L Y, Huang J W, Yuan H T, Titov A N, Eriksson O and Ong C S 2024 *Nano Lett.* **24** 5562

[33] Gao Y P, Tian C, Huang X L, Wang X and Cui T 2024 *Phys. Rev. B* **109** 104501

[34] Island J O, Molina-Mendoza A J, Barawi M, Biele R, Flores E, Clamagirand J M, Ares J R, Sánchez C, van der Zant H S J, D'Agosta R, Ferrer I J and Castellanos-Gomez A 2017 *2D Mater.* **4** 022003

[35] Balandin A A, Kargar F, Salguero T T and Lake R K 2022 *Mater. Today* **55** 74

[36] Yue B B, Zhong W, Deng W, Wen T, Wang Y G, Yin Y Y, Shan P F, Wang J T, Yu X H and Hong F 2023 *J. Am. Chem. Soc.* **145** 1301

[37] Yue B B, Zhong W, Zhang H, Zhou J, Miao J W, Kawaguchi S, Kadobayashi H and Hong F 2024 *Phys. Rev. B* **110** 144515

[38] Yu H, Yan D Y, Guo Z P, Zhou Y Z, Yang X, Li P L, Wang Z J, Xiang X J, Li J K, Ma X L, Zhou R, Hong F, Wuli Y X, Shi Y G, Wang J T and Yu X H 2024 *J. Am. Chem. Soc.* **146** 3890

[39] Keszler D A, Squattrito P J, Brese N E, IBERS J A, Shang M Y and Lu J X 1985 *Inorg. Chem.* **24** 3063

[40] Liu W H, Feng J J, Hou Q, Li B, Wang K, Chen B, Li S and Shi Z X 2024 *Phys. Rev. B* **109** 054513

[41] Yang H Y, Zhou Y H, Li L Y, Chen Z, Zhang Z Y, Wang S Y, Wang J, Chen X L, An C and Zhou Y 2022 *Phys. Rev. Mater.* **6** 084803

[42] Gressier P., Meerschaut A., Guemas L., Rouxel J. and Monceau P. 1984 *J. Solid State Chem.* **51** 141

[43] An C, Zhou Y H, Chen C H, Fei F C, Song F Q, Park C R, Zhou J H, Rubahn H G, Moshchalkov V V, Chen X L, Zhang G F and Yang Z R 2020 *Adv. Mater.* **32** 2002352

[44] Pei C, Shi W, Zhao Y, Gao L, Gao J, Li Y, Zhu H, Zhang Q, Yu N, Li C, Cao W, Medvedev S A, Felser C, Yan B, Liu Z, Chen Y, Wang Z and Qi Y 2021 *Mater. Today Phys.* **21** 100509

[45] Sipos B, Kusmartseva A F, Akrap A, Berger H, Forro L and Tutis E 2008 *Nat. Mater.* **7** 960

[46] Chang J, Blackburn E, Holmes A T, Christensen N B, Larsen J, Mesot J, Liang R X, Bonn D A, Hardy W N, Watenphul A, Zimmermann M v, Forgan E M and Hayden S M 2012 *Nat. Phys.* **8** 871

[47] Yu F H, Ma D H, Zhuo W Z, Liu S Q, Wen X K, Lei B, Ying J J and Chen X H 2021 *Nat. Commun.* **12** 3645

[48] Lou R, Cai Y P, Liu Z H, Qian T, Zhao L X, Li Y, Liu K, Han Z Q, Zhang D D, He J B, Chen G F, Ding H and Wang S C 2016 *Phys. Rev. B* **93** 115133

[49] Kogar A, de la Pena G A, Lee S J, Fang Y, Sun S X L, Lioi D B, Karapetrov G, Finkelstein K D, Ruff J P C, Abbamonte P and Rosenkranz S 2017 *Phys. Rev. Lett.* **118** 027002

[50] Hamlin J J, Zocco D A, Sayles T A, Maple M B, Chu J H and Fisher I R 2009 *Phys. Rev. Lett.* **102** 177002

[51] Feng J J, Susilo R A, Lin B C, Deng W, Wang Y j, Li B, Jiang K, Chen Z Q, Xing X Z, Shi Z X, Wang C L and Chen B 2020 *Adv. Electron. Mater.* **6** 1901427

[52] Wang S Y, Wang Q, An C, Zhou Y H, Zhou Y, Chen X L, Hao N and Yang Z R 2023 *Matter* **6** 3526

[53] Liu Z Y, Li J, Zhang J F, Li J, Yang P T, Zhang S, Chen G F, Uwatoko Y, Yang H X, Sui Y, Liu K and Cheng J G 2021 *npj Quantum Mater.* **6** 90

[54] Briggs A, Monceau P, Nunez Regueiro M, Peyrard J, Ribaultl M and Richard J 1980 *J. Phys. C: Solid State Phys.* **13** 2117

[55] Ido M, Okayama Y, Ijiri T and Okajima Y 1990 *J. Phys. Soc. Jpn.* **59** 1341

[56] Monteverde M, Lorenzana J, Monceau P and Núñez-Regueiro M 2013 *Phys. Rev. B* **88** 180504(R)

[57] Gleason S L, Gim Y, Byrum T, Kogar A, Abbamonte P, Fradkin E, MacDougall G J, Van Harlingen D J, Zhu X D, Petrovic C and Cooper S L 2015 *Phys. Rev. B* **91** 155124

[58] Yamaya K, Yoneda M, Yasuzuka S, Okajima Y and Tanda S 2002 *J. Phys.: Condens. Matter* **14** 10767

[59] Yamamoto M 1978 *J. Phys. Soc. Jpn.* **45** 431

[60] Yamaya K, Geballe T H, Kwak J F and Greene R L 1979 *Solid State Commun.* **31** 627

[61] Cai Y K, Zhang C T, Cao T C, Feng J J, He Z, Xing X Z, Liu X B, Shi Z X, Qian B and Zhou W 2024 *Phys. Rev. B* **110** 094516

[62] Yang X C, Luo X, Gao J J, Jiang Z Z, Wang W, Wang T Y, Si J G, Xi C Y, Song W H and Sun Y P 2021 *Phys. Rev. B* **104** 155106

[63] Zhang J, Jia Y T, Wang X C, Li Z, Duan L, Li W M, Zhao J F, Cao L P, Dai G Y, Deng Z, Zhang S J, Feng S M, Yu R Z, Liu Q Q, Hu J P, Zhu J L and Jin C Q 2019 *NPG Asia Mater.* **11** 60

[64] Qi Y P, Shi W J, Werner P, Naumov P G, Schnelle W, Wang L, Rana K G, Parkin S, Medvedev S A, Yan B H and Felser C 2018 *npj Quantum Mater.* **3** 4

[65] Li X, Chen D Y, Jin M L, *et al*. 2019 *Proc. Natl. Acad. Sci. USA* **116** 17696

[66] Feng J J, Chen Z C, Fan Y J, Yang M, Zhuang J C, Liu J Y, Wang M H, He Z, Guo H T, Qian B, Shi Z X and Zhou W 2023 *Supercond. Sci. Technol.* **36** 085010

[67] Xu S X, Liu Z Y, Yang P T, Ruan B B, Ren Z A, Sun J P, Uwatoko Y, Wang B S and Cheng J G 2024 *Phys. Rev. B* **109** 144107

[68] Xu F and Zhang L 2024 *Chin. Phys. B* **33** 037402

[69] Liu R H, Wu G, Wu T, Fang D F, Chen H, Li S Y, Liu K, Xie Y L, Wang X F, Yang R L, Ding L, He C, Feng D L and Chen X H 2008 *Phys. Rev. Lett.* **101** 087001

[70] Rullier-Albenque F, Colson D, Forget A and Alloul H 2009 *Phys. Rev. Lett.* **103** 057001

[71] Chen H, Ren Y, Qiu Y, Bao W, Liu R H, Wu G, Wu T, Xie Y L, Wang X F, Huang Q and Chen X H 2009 *EPL* **85** 17006

[72] Li Z, Zhou R, Liu Y, Sun D L, Yang J, Lin C T and Zheng G Q 2012 *Phys. Rev. B* **86** 180501(R)

[73] Takahashi H, Sugimoto A, Nambu Y, Yamauchi T, Hirata Y, Kawakami T, Avdeev M, Matsubayashi K, Du F, Kawashima C, Soeda H, Nakano S, Uwatoko Y, Ueda Y, Sato T J and Ohgushi K 2015 *Nat. Mater.* **14** 1008

[74] Yamauchi T, Hirata Y, Ueda Y and Ohgushi K 2015 *Phys. Rev. Lett.* **115** 246402

[75] Caron J M, Neilson J R, Miller D C, Llobet A and McQueen T M 2011 *Phys. Rev. B* **84** 180409(R)

[76] Mourigal M, Wu S, Stone M B, Neilson J R, Caron J M, McQueen T M and Broholm C L 2015 *Phys. Rev. Lett.* **115** 047401

[77] Zheng L L, Frandsen B A, Wu C W, Yi M, Wu S, Huang Q Z, Bourret-Courchesne E, Simutis G, Khasanov R, Yao D X, Wang M and Birgeneau R J 2018 *Phys. Rev. B* **98** 180402(R)

[78] Ying J J, Lei H C, Petrovic C, Xiao Y M and Struzhkin V V 2017 *Phys. Rev. B* **95** 241109(R)

[79] Du F, Ueda Y and Ohgushi K 2019 *Phys. Rev. Lett.* **123** 086601

[80] Imaizumi S, Aoyama T, Kimura R, Sasaki K, Nambu Y, Avdeev M, Hirata Y, Ikemoto Y, Moriwaki T, Imai Y and Ohgushi K 2020 *Phys. Rev. B* **102** 035104
[81] Yu J, Wang M, Frandsen B A, Sun H L, Yin J J, Liu Z J, Wu S, Yi M, Xu Z J, Acharya A, Huang Q Z, Bourret-Courchesne E, Lynn J W and Birgeneau R J 2020 *Phys. Rev. B* **101** 235134
[82] Fan Y J, Liu J Y, Feng J J, Chen Z C, Wang M H, He Z, Guo H T, Qian B, Shi Z X and Zhou W 2022 *Supercond. Sci. Technol.* **35** 085007
[83] Takahashi H, Kikuchi R, Kawashima C, Imaizumi S, Aoyama T and Ohgushi K 2022 *Materials* **15** 1401
[84] Zhang Y, Lin L F, Zhang J J, Dagotto E and Dong S 2018 *Phys. Rev. B* **97** 045119
[85] Bao J K, Liu J Y, Ma C W, Meng Z H, Tang Z T, Sun Y L, Zhai H F, Jiang H, Bai H, Feng C M, Xu Z A and Cao G H 2015 *Phys. Rev. X* **5** 011013
[86] Tang Z T, Bao J K, Liu Y, Sun Y L, Ablimit A, Zhai H F, Jiang H, Feng C M, Xu Z A and Cao G H 2015 *Phys. Rev. B* **91** 020506(R)
[87] Tang Z T, Bao J K, Wang Z, Bai H, Jiang H, Liu Y, Zhai H F, Feng C M, Xu Z A and Cao G H 2015 *Sci. China Mater.* **58** 16
[88] Sun J P, Jiao Y Y, Yang C L, Wu W, Yi C J, Wang B S, Shi Y G, Luo J L, Uwatoko Y and Cheng J G 2017 *J. Phys. Condens. Matter* **29** 455603
[89] Wang Z, Yi W, Wu Q, Sidorov V A, Bao J K, Tang Z T, Guo J, Zhou Y Z, Zhang S, Li H, Shi Y G, Wu X X, Zhang L, Yang K, Li A G, Cao G H, Hu J P, Sun L L and Zhao Z X 2016 *Sci. Rep.* **6** 37878
[90] Liu Z Y, Mu Q G, Ren Z A, Sun J P and Cheng J G 2023 *Sci. Sin., Phys., Mech. Astron.* **53** 127417
[91] Kong T, Bud'ko S L and Canfield P C 2015 *Phys. Rev. B* **91** 020507(R)
[92] Xiang J J, Yu Y L, Wu S Q, Li B Z, Shao Y T, Tang Z T, Bao J K and Cao G H 2019 *Phys. Rev. Mater.* **3** 114802
[93] Li B Z, Wu S Q, Xiang J J, Zhu Q Q, Liu Y, Cao C and Cao G H 2023 *Sci. China Phys, Mech. Astron.* **66** 237411
[94] Liu Z Y, Dong Q X, Yang P T, Shan P F, Wang B S, Sun J P, Dun Z L, Uwatoko Y, Chen G F, Dong X L, Zhao Z X and Cheng J G 2022 *Phys. Rev. Lett.* **128** 187001
[95] Yang P T, Dong Q X, Shan P F, Liu Z Y, Sun J P, Dun Z L, Uwatoko Y, Chen G F, Wang B S and Cheng J G 2022 *Chin. Phys. Lett.* **39** 067401
[96] Long S J, Chen L, Wang Y X, Zhou Y, Cai S, Guo J, Zhou Y Z, Yang K, Jiang S, Wu Q, Wang G, Hu J P and Sun L L 2022 *Phys. Rev. B* **106** 214515
[97] Shan P F, Dong Q X, Yang P T, Xu L, Liu Z Y, Shi L F, Wang N N, Sun J P, Uwatoko Y, Chen G F, Wang B S and Cheng J G 2023 *Phys. Rev. B* **107** 094519
[98] Zhou Y, Chen L, Zhao L L, Long S J, Wang Y X, Qiu X L, Chai C C, Guo Z N, Zhang Q H, Guo J, Liu K, Lin Q S, Sun L L, Hu J P and Wang G 2023 *Sci. Sin., Phys., Mech. Astron.* **53** 127413